

# Predictive Fuel Dynamic Control During Engine Start and Crank-to-Run Transition for Port Fuel Injected Gasoline Engines

Qi Ma, Stephen Yurkovich, and Kenneth P. Dudek

**Abstract**—Automotive emission regulations have sharply increased the calibration effort required to tune conventional fuel control algorithms for engine start and crank-to-run transition. This paper presents a model-based control approach with predictive fuel dynamics control that mitigates some of the calibration effort. Instead of using a static equivalence ratio blending approach to compute the fuel command during start and crank-to-run transition, the method suggests using scheduled in-cylinder fresh air charge prediction, individual cylinder fuel dynamics compensation (via direct inversion of a fuel dynamics model), and lost fuel correction. Misfire and poor starts are detected and mitigated using intelligent mode scheduling of the in-cylinder fresh air charge predictor, which includes special modes for misfire and poor start. The result is fault tolerant predictive fuel control, even in the face of misfire or poor starts. The scheme has been validated on production L4 and V8 engines over a wide range of operating conditions, and the paper presents selected results from that validation study.

## I. INTRODUCTION

Obtaining a robust start for a Port Fuel Injected (PFI) automotive engine, while simultaneously minimizing hydrocarbon (HC) emission under all start conditions, is challenging for automotive manufacturers. The difficulties arise from the complex physics of the plant, the impact that varying fuel composition has on fuel compensation, a dearth of accurate measurements of key physical quantities, and the lack of a simple and accurate mathematical math model for the problem. These difficulties are compounded by the extremely short duration of the transition and huge change in operating condition as the engine accelerates from cranking speed to (high) idle speed. Moreover, in order to minimize HC emission, automobile manufacturers usually inject fuel at the earlier possible event because this maximizes the amount of time that the injected fuel has to vaporize before being ingested into the cylinder. This fuel must be calculated and delivered long before the charge is ingested into the cylinders. These factors have prevented the identification of reliable control-oriented models for fuel control in the start and crank-to-run regime of engine operation [10].

Traditionally, fuel control for engine start and crank-to-run transition featured simple algorithms that shaped the fuel command based on simple heuristics. One common approach multiplies estimates of current cylinder air mass by an equivalence ratio (EQR) that is a blend of an EQR appropriate for engine crank and another that is appropriate for engine run. Increasingly rigorous emission requirements,

S. Yurkovich is with the Center for Automotive Research at The Ohio State University.

Q. Ma and K. P. Dudek are with General Motors Powertrain Advanced Engineering.

however, led to increasing flexibility in these heuristics, usually in the form of more crank EQR tables (based on more variables) or more complicated factors to "blend" the crank and run EQRs. These methods permit calibrators to adjust the shape of the fuel command in increasingly complex ways. Unfortunately, the complexity of these enhanced methods became difficult (and expensive) to calibrate.

Competition in the global automobile market is intense. All manufacturers are under pressure to decrease costs while increasing quality. Model-based control methods can help with these pressures because they can decrease the cost and increase the quality of engine control calibrations. Unsurprisingly, manufacturers began adopting model-based control methods in the 1990's (see [6], [7], [5], [3]). This trend also included the engine start problem [9], although much of the work on model-based controls for engine start did not appear until later (see [10], [11], [12]). Moreover, certain critical aspects of the underlying physical phenomena have been under study simultaneously ([16], [15], [9], [13]). One of the more interesting, recent developments is the documentation of "fuel loss" (i.e., incomplete fuel utilization phenomenon) during start and crank-to-run ([2], [8], [14]), and a "diminishing return" effect associated with compensation for this lost fuel ([10] and [11]).

This paper builds on the authors previously reported results to present a complete picture of model-based, predictive, individual cylinder fuel control for engine start and crank-to-run. The paper is organized as follows. Section II gives the general architecture of predictive fuel dynamics control for the engine start problem. Section III surveys the family of air prediction models that underpin the solution, while Section IV details nominal fuel dynamics control. Section V formulates the lost fuel compensation. Section VI discusses calibration methods, and Section VII presents selected experimental results. Conclusions and suggestions for future work appear in Section VIII.

## II. PREDICTIVE FUEL DYNAMICS CONTROL

The architecture of predictive fuel dynamics control developed in this work is depicted in Figure 1. As shown,

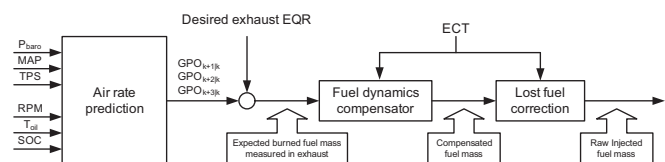


Fig. 1. Architecture of predictive fuel dynamics control

the predictive fuel dynamics control consists of four main components:

- 1) Multi-Step Cylinder Air Mass Prediction: Due to event-based fuel control and the PFI configuration, the cylinder air mass must be predicted up to three steps ahead for Line-4 (L4) engines and seven steps ahead for V8 engines (measured by the number of engine events) for fuel command calculation.
- 2) Nominal Fuel Dynamics Compensator: This component is essentially a direct inverse of the nominal fuel dynamics model; with this configuration, open loop control is designed to achieve approximate unity gained response.
- 3) Inverse Utilized Fuel Fraction (UFF): By inverting the forward UFF function [11], the output of the nominal fuel dynamics controller is corrected to compensate the lost fuel effect. Together with the nominal fuel dynamics compensator, the inverse UFF function realizes a control such that, by compensating the lost fuel effect, the measured exhaust EQR is very close to the commanded EQR measurement.
- 4) Desired Exhaust EQR: This element gives several flexible choices in the control calibration process such as meeting different emission requirements and plug fouling prevention.

Though readily conceived as an open loop fuel dynamics compensation scheme (Figure 1), such an architecture, used during engine start and crank-to-run transition, is quite powerful. Due to the unique characteristics of the problem and the practical implication of the solution, we have very little to compare our results against in this work.

### III. CYLINDER AIR MASS PREDICTION

Based on several phases experienced by PFI engines during starts, the cylinder air mass model is partitioned based on the phase or state of the engine speed. Among three

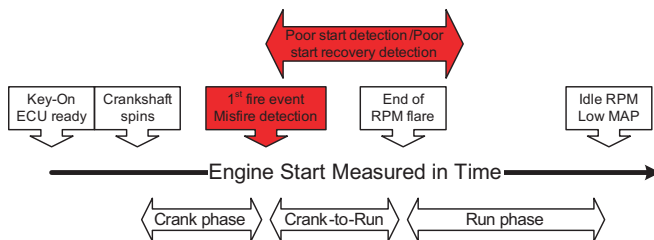


Fig. 2. Three phases in a typical engine start.

phases and the misfire mode as shown in Figure 2, crank phase and crank-to-run phase play a key role in a successful engine start. Due to the main emphasis in this work, the run phase cylinder air mass model and predictor design will not be discussed. In the rest of this section, cylinder air mass models and corresponding predictors are presented.

#### A. Cylinder Air Mass Models

For the sake of notational convenience, in this work models are given in term of the cylinder air mass,  $GPO$  [12].

1) *Crank GPO Model*: Similar to the crank GPO model used in [12], the cylinder air mass dynamics can be accurately described by the following model:

$$GPO(k+1) = \alpha_{CRK} GPO(k). \quad (1)$$

In the above expression,  $\alpha_{CRK}$  is a linear spline function [4] of throttle position and can be identified by least squares algorithm. We note that Equation (1) is slightly different from the one used in [12]. It is believed that, for engines with fast engine synchronization hardware [10], air steady state may not be achievable prior to the first firing event where the decay rate is much larger; therefore, Equation (1) is sufficient. In certain engine configurations, such as in some engine platforms where the throttle opening is relatively large during cranking,  $\alpha$  can be a single number rather than a function of the throttle position.

2) *Crank-to-Run GPO Model*: The experimental data [12] indicates that a first order autonomous decay model would be sufficient for the engine crank-to-run phase, with a decay rate dependent on throttle position (TPS) and RPM, given by

$$GPO(k+1) = \alpha_{CTR}(TPS(k), RPM(k)) GPO(k), \quad (2)$$

where the crank-to-run transition linear spline function  $\alpha_{CTR}$  is given by

$$\alpha_{CTR}(TPS(k), RPM(k)) = K_0 + \sum_{i=1}^m K_i TPS_i(k) + \sum_{j=1}^n K_{m+j} RPM_j(k). \quad (3)$$

In this linear spline expression,  $TPS_i(k)$  and  $RPM_j(k)$  are linear spline basis functions. The coefficients ( $K_i$ ) in Equations (3) can be identified robustly by least squares algorithms [1], given sufficient measurements.

Regarding air prediction in case of misfire, as discussed extensively in [10], air dynamics during misfire or poor start cases usually exhibit sporadic patterns. In later sections, a simple method is given to predict cylinder air mass under misfire, while ensuring a sufficient degree of robustness for the control.

#### B. Multi-Step Cylinder Air Mass Predictor

Multi-step prediction is a direct consequence of event based engine control in multi-cylinder engines. For Instance, in order to fuel a production V8 engine at  $-30^\circ\text{C}$ , fuel must be delivered at least seven events ahead of its BDC (Bottom Dead Center) intake event, so as to maximize fuel residence time. However, in the next seven engine events, the cylinder air mass may experience two different modes based on the location of the first power event, thus appropriate prediction scheduling is required, given engine position information.

First of all, a scheduled cylinder air mass filter is presented which is required to handle abnormalities in the face of engine misfire and poor start.

1) *Scheduled GPO Filter*: A scheduled GPO filter for GPO measurement is implemented during all three phases in

an engine start; the two equations associated with the GPO filter are:

$$GPOF(k) = GPOF(k-1) + (0.9)(GPOM(k) - GPOF(k-1)) \quad (4)$$

$$GPOF(k) = GPOF(k-1) + (0.1)(GPOM(k) - GPOF(k-1)) \quad (5)$$

If abnormalities are detected, Equation (5) is used to filter the raw measurement  $GPOM$ ; otherwise Equation (4) is used. In the above expressions, the GPO measurement at event  $k$ ,  $GPOM(k)$ , is calculated using

$$GPOM(k) = VE_{CRK} \frac{MAP(k)}{IAT(k)}, \quad (6)$$

where  $IAT$  is the intake air temperature, and  $VE_{CRK}$  is the volumetric efficiency at the cranking speed, usually taking a single fixed number for all engine start conditions. The detailed assessment can be found in [10].

2) *Crank GPO Predictor*: The crank GPO predictor consists of 1<sup>st</sup> step ahead up to  $i$ -<sup>th</sup> step ahead GPO predictions. The equation associated with the crank GPO predictor is summarized below:

$$GPO(k+i|k) = \alpha_{CRK} GPO(k-1+i|k). \quad (7)$$

where

$$GPO(k|k) = GPO(k-1|k) + L(GPOF(k) - GPO(k-1|k))$$

and the notation  $GPO(k+i|k)$ , means, “ $i$ -th step GPO prediction given information at event  $k$ ”, and  $L$  denotes the estimator gain. The subscript “ $CRK$ ” in the parameter,  $\alpha_{CRK}$ , denotes a “*crank*” condition.

3) *Crank-to-Run GPO Predictor*: Similar to the crank cylinder air mass predictor, the crank-to-run GPO predictor consists of 1<sup>st</sup> step ahead up to  $i$ -<sup>th</sup> step ahead GPO predictions and measurement update. The equation associated with the crank-to-run GPO predictor is summarized below:

$$GPO(k+i|k) = \alpha_{CTR} GPO(k-1+i|k) \quad (8)$$

The predictor coefficient  $\alpha_{CTR}$ , where subscript “ $CTR$ ” denotes “*crank-to-run*” condition, is a linear spline function of TPS and engine RPM signals:

$$\alpha_{CTR}(k) = K_0 + \sum_{i=1}^m (K_i) TPS_i(k) + \sum_{j=1}^n (K_{m+j}) RPM_j(k). \quad (9)$$

As before, the notation  $GPO(k+i|k)$ , means, “ $i$ -<sup>th</sup> step ahead GPO prediction given information at event  $k$ ”. The measurement update equation for the crank-to-run predictor is

$$GPO(k|k) = GPO(k-1|k) + L(GPOF(k) - GPO(k|k-1)), \quad (10)$$

where  $L$  denotes the estimator gain.

4) *Misfire/Poor-Start GPO Predictor*: Whenever misfire or poor start is detected in an engine start, the mode of the

filtered GPO is scheduled accordingly. The GPO prediction is carried out according to the following rules:

$$GPO(k+i|k) = \alpha_{m,p} GPO(k|k) \quad (11)$$

The parameter,  $\alpha_{m,p}$ , denotes a GPO decay rate in the cases of misfire (subscript  $m$ ) or poor-start (subscript  $p$ ), and can be hand-tuned (calibrated). The measurement update equation for the misfire/poor-start GPO predictor is

$$GPO(k|k) = GPO(k-1|k) + L(GPOF(k) - GPO(k|k-1)), \quad (12)$$

where  $L$  denotes the estimator gain. The detailed rules and formulas to set these estimator gains are given in [10].

### C. Air Prediction Scheduling and Assignment

When air prediction starts from the first step ahead prediction, a rule is required to decide which air predictor should be in place: crank air predictor, crank-to-run air predictor or misfire air predictor. Generally speaking, as the engine event marches toward the first firing event, less air prediction is made by the crank air predictor and the crank-to-run predictor will gradually take over. Also, when  $N$  step ahead air predictions are made, either from the crank or crank-to-run predictor, each of them must be assigned to the correct cylinders. In [12], a simple rule is depicted graphically from each event instance of view. In this work, a comprehensive view is given to help understand the scheduling and assignment rule (Figure 3). As shown in Figure 3, the basic

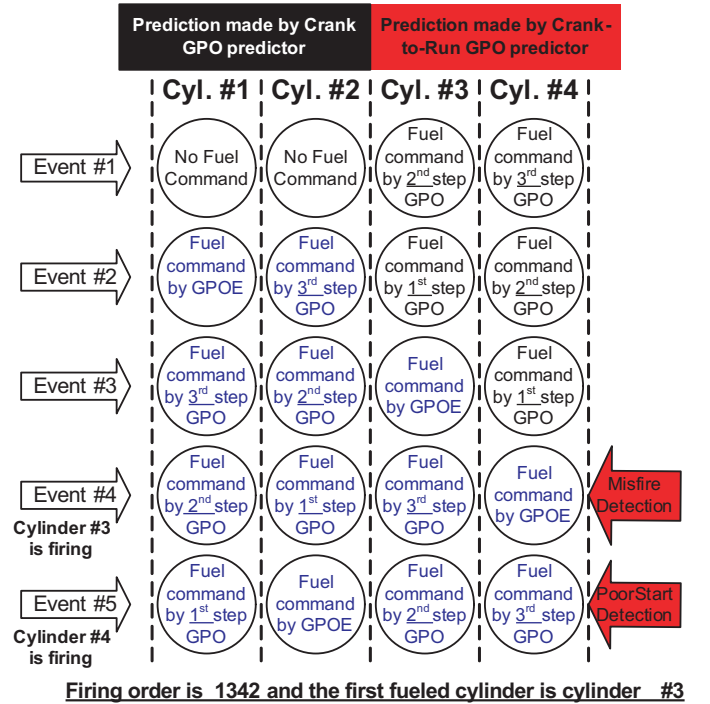


Fig. 3. Assignment of air prediction for a four-cylinder engine

theme behind the picture is that each cylinder will have fuel commanded  $N-1$  times in each fuel cycle, if the prediction

horizon is  $N$  steps-ahead<sup>1</sup>. The fuel delivery hardware will pick the correct fuel command to use based on engine speed and the end of inject target.

#### IV. FUEL DYNAMICS CONTROL

With a good prediction of future cylinder air mass in hand, what remains to solve the start control problem is a scheme for fuel dynamics control.

##### A. Nominal Fuel Dynamics Model

Motivated by observations in real engine data [11], the fuel dynamics model structure is selected to take the first order discrete  $\tau$ - $X$  model form, but the coefficients are scheduled according to the engine coolant temperature (ECT); that is,

$$m_{dep}(k) = (1 - \tau)m_{dep}(k-1) + (1 - X)m_{cinj}(k) \quad (13)$$

$$m_{cyl}(k) = \tau m_{dep}(k-1) + X m_{cinj}(k) \quad (14)$$

In the above expression,  $m_{dep}$  refers to the deposited fuel mass on the surface of the fuel pass, such as the intake valve, top of piston and cylinder wall;  $m_{cyl}$  refers to the true fuel mass in vapor form which participates in the combustion process and is measured by MBFM<sup>2</sup>; and  $m_{cinj}$  is the CINJ<sup>3</sup>.

With the above formulation, at engine start conditions, the quantity of the first cycle in-cylinder fuel mass is dictated mainly by the parameter  $X$  and UFF:

$$m_{cyl}(1) = MBFM(1) = (X)UFF(RINJ(1))RINJ(1). \quad (15)$$

In the above, RINJ denotes the Raw Injected Fuel Mass. The formula of calculating CINJ will be given in the next section. Due to the nonlinear coupling between UFF and the nominal fuel dynamics, there are some issues regarding model calibration, discussed extensively in [10]. Due to one-to-one correspondence of the  $\tau$ - $X$  model and the ARMA model, the nominal fuel dynamics can be written in the following from:

$$y(k) = -\beta_1(ECT)y(k-1) + \alpha_0(ECT)u(k) + \alpha_1(ECT)u(k-1), \quad (16)$$

with several new variables and parameters defined. Though both discrete models are equivalent, they are used simultaneously in the model calibration process.

##### B. Individual Cylinder Fuel Dynamics

By inverting the above equation, the nominal fuel dynamics compensator is obtained:

$$u(k) = -\frac{\alpha_1}{\alpha_0}u(k-1) + \frac{1}{\alpha_0}y(k) + \frac{\beta_1}{\alpha_0}y(k-1), \quad (17)$$

where  $y(k)$  and  $u(k)$  become commanded MBFM and commanded CINJ (compensator output), respectively. It is worth noting that the above equation is used for fueling only one cylinder; the remaining cylinders are treated identically

<sup>1</sup>Usually,  $N$  is the number of cylinders in the engine.

<sup>2</sup>MBFM denotes the Measured Burned Fuel Mass derived from cylinder air mass measurement and wide band exhaust air-fuel-ratio sensor.

<sup>3</sup>CINJ denotes lost fuel Corrected Raw Injected Fuel Mass.

but with different current and past fuel commands and compensator outputs. In other words, the following equation is actually used in the nominal fuel dynamics control for V8 engines:

$$u_{cyl,i}(k) = -\frac{\alpha_1}{\alpha_0}u_{cyl,i}(k-1) + \frac{1}{\alpha_0}y_{cyl,i}(k) + \frac{\beta_1}{\alpha_0}y_{cyl,i}(k-1), \quad (18)$$

where  $i$  takes a value from 1 to 8. Details of initializing this individual nominal fuel dynamics control for each cylinder and its implication can be found in [10].

#### V. LOST FUEL COMPENSATION

One factor that makes fuel control for PFI engines during start and crank-to-run so difficult is the "lost fuel" effect shown in Figure 4. The difference between raw injected fuel (RINJ) and measured, burned fuel (MBFM) is either stored in the engine (in the oil!) or it escapes, unburned, through the exhaust. The inefficient fuel utilization persists when the

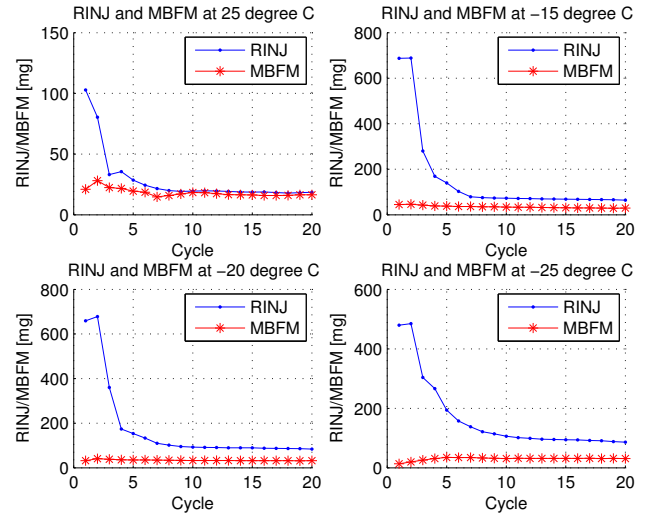


Fig. 4. RINJ vs. MBFM at four different ECTs

engine is not fully warmed up. The stored portion of the "lost fuel" mass will eventually appear in the output measurement, but not in the time window of interest. To compensate the lost fuel, fuel enrichment at the start is inevitable, and properly enriching the fuel will require a lost fuel model.

##### A. Lost Fuel Model

Although the open literature offers no direct indication about the precise form of the nonlinearity required in the nonlinear Utilized Fuel Fraction (UFF) formation, some possible directions may be gleaned after several trials for different functional forms. The following form is chosen in this work:

$$CINJ = UFF_{ss}(ECT) \times \left( 1 - \frac{2}{\pi} \arctan \left( \frac{RINJ}{\gamma(ECT)} \right) \right) RINJ, \quad (19)$$

where  $UFF_{ss}$  and  $\gamma$  are ECT dependent scalar functions. The UFF is therefore defined as

$$UFF = \frac{CINJ}{RINJ} = UFF_{ss}(ECT) \left( 1 - \frac{2}{\pi} \arctan \left( \frac{RINJ}{\gamma(ECT)} \right) \right). \quad (20)$$

The basic correction characteristic of the UFF, which focuses on the diminishing return effect along with increased RINJ, is depicted in Figure 5.

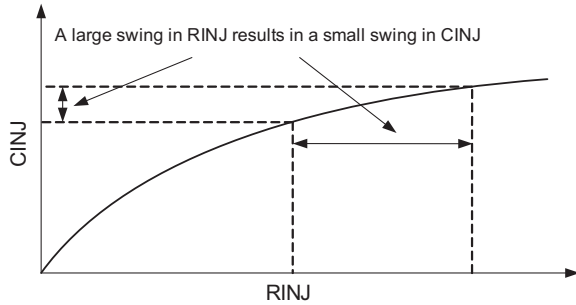


Fig. 5. Diminishing Return Effect of UFF function.

Moreover, as reported in [8], the fuel utilization phenomena appears to be unique for Cycle 1 and Cycle 2. For this paper, however, Cycle 1 and Cycle 2 are treated identically for a given ECT. Hence,

$$CINJ(1) = UFF_{C1} \times RINJ(1) \quad (21)$$

$$CINJ(2) = UFF_{C1} \times RINJ(2) \quad (22)$$

where  $UFF_{C1}$  is the UFF for Cycle 1.

### B. Lost Fuel Function Inverse

By construction, the UFF model is a smooth function with a saturation limit. When used directly in control, it is possible to specify a (large) commanded CINJ which may not have a corresponding value of RINJ. Without modification, this cannot be implemented in control.

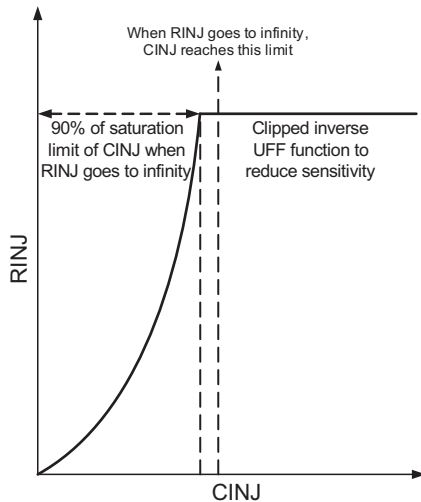


Fig. 6. Clipped output of the inverse UFF function.

To overcome this incomplete mapping issue when inverting UFF in control, the output of the inverse UFF function is clipped as shown in Figure 6. The modified inverse UFF function is comprised of two components: 1) the saturation limit; and 2) implementation of numerical inversion. Even with such an approach, a sensitivity issue arises when inverting the UFF function for control, as depicted in Figure 7 (heavy dashed curve). With Cycle 1 and Cycle 2 UFF,

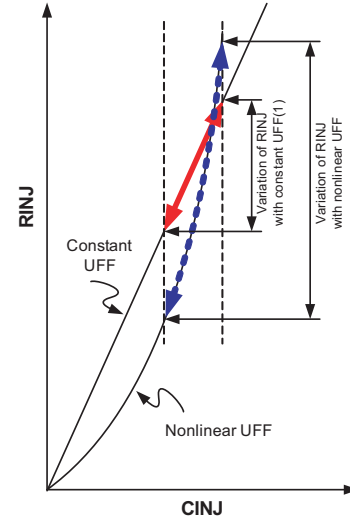


Fig. 7. Advantage of independent  $UFF_{C1}$  over nonlinear UFF function

the sensitivity issue can be drastically reduced in the case of abnormal engine start. Detailed setting of this inverse function can be found in [10] and [11].

## VI. CONTROL CALIBRATION

Because air prediction calibration has been elucidated in [10] and [12], fuel control calibration is described in this section.

The calibration procedure of the  $UFF_{ss}(ECT)$  curve is simple: carry out a quadratic or cubic polynomial curvefit given several  $UFF_{ss}$  measurements at each representative ECT with one special treatment that the output of the regressed function is saturated at "1". The UFFs function on a typical V8 engine is depicted in Figure 8.

Regarding identifying the UFF and nominal fuel dynamics models ( $\tau$  and  $X$ ), a special optimization routine is designed to identify UFF and fuel dynamics simultaneously. A multi-step calibration process for  $\gamma(ECT)$  and the nominal fuel dynamics model are obtained through a joint optimization routine implemented with the following iteration steps as shown in Figure 9. Parameter  $R$ , shown in the second step of the inner loop of Figure 9, is calculated by the following formula:

$$R \approx \frac{\sum_{k=1}^{20} u(k) - \sum_{k=1}^{20} m_{cyl}(k)}{\frac{1}{5} \sum_{k=16}^{20} m_{cyl}(k)}. \quad (23)$$

The advantage of using parameter  $R$  to identify fuel dynamics parameters is well explained in [10]. Also, parameter  $\tau$  shown in the inner loop of the joint optimization is the evaporation rate of " $\tau - X$ " model (Equation 13).

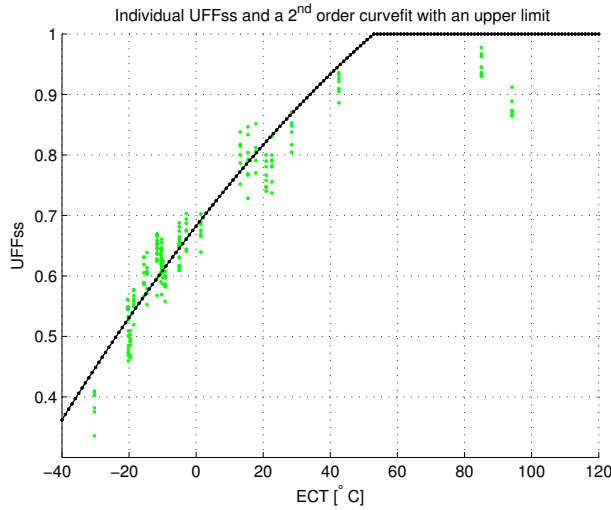


Fig. 8. The regressed  $UFF_{ss}(ECT)$  function with saturation limit. The  $UFF_{ss}$  is the ratio of the measured burned fuel mass and the raw injected fuel mass around 20th fuel cycle of each cylinder.

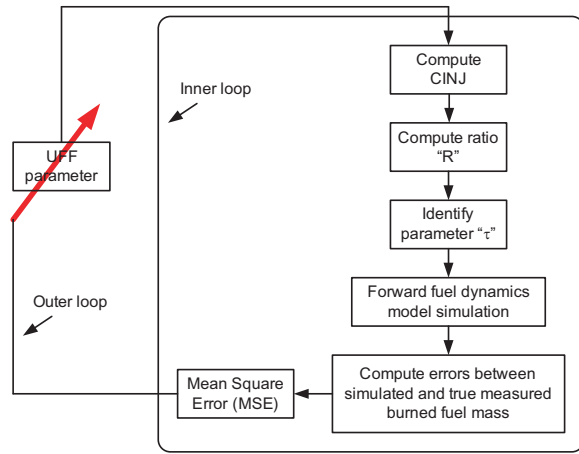


Fig. 9. Joint optimization for  $\gamma(ECT)$ ,  $UFF_{C1}$  and nominal fuel dynamics

## VII. EXPERIMENTAL RESULTS

When the earlier work [10], [11], [12] was developed, the predictive fuel control scheme was mainly focused on production L4 engines, though with consideration of application to L5, V6 and V8 engines. Over the last two years, the scheme has been refined and expanded to cover all types of production engines. Although validated on both L4 and V8 engines, in this work, validation results from a production V8 engine are given. For readers who are interested in validation results of L4 engines, [12] supplied some offline air prediction validation results. Validation data for L4 engines may appear in a future report.

### A. Air Prediction Performance

During engine start and crank-to-run transition, the first few air predictions are crucial. As shown in Figure 10, air prediction performs well, especially during first couple engine events. Each of the curves in Figure 10 show successive

cylinder air mass predictions on the same cylinder, demonstrating the accuracy of the multi-step prediction method.

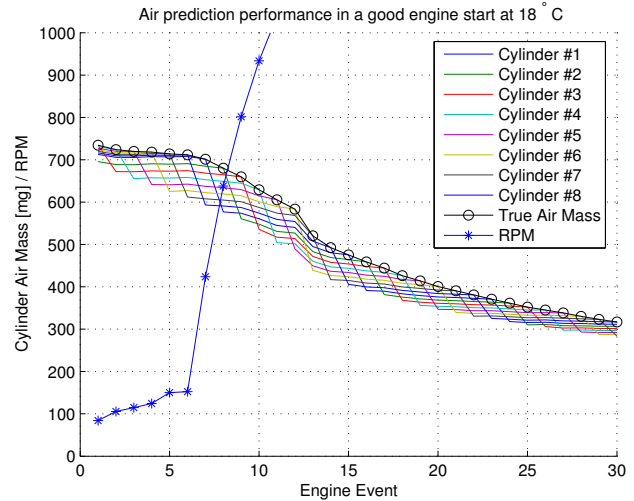


Fig. 10. Air prediction performance in a good engine start: The first firing event occurs at event #7. With CVI settings for V8 engines, the earliest firing event is at Event #7 if engine position is perfectly known at the beginning.

Figure 11 gives a close-up view of Figure 10, it is clear that, even for the first one or two events, the air prediction scheme gives close air prediction for run speed events when the engine is still at cranking speed.

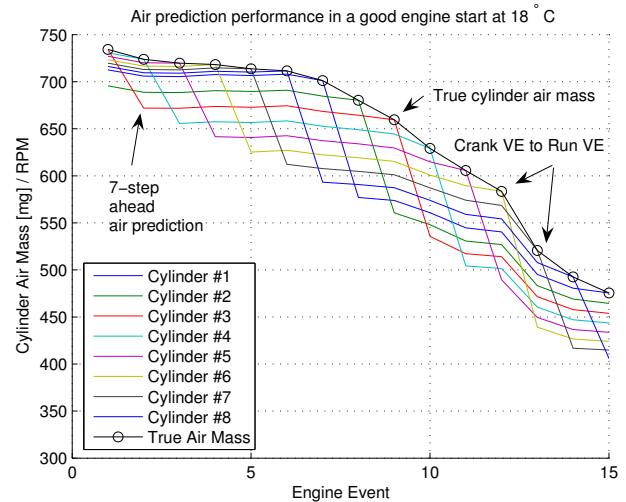


Fig. 11. The 7-step ahead air prediction calculated at the second engine event is very close to true cylinder air mass in a good engine start.

Figure 12 shows what happens when misfire is detected. All air predictions are forced to the same value: that of the first step ahead prediction, by using the misfire air predictor. A close-up view is shown in Figure 13.

When the engine RPM is fully recovered from misfire, all air predictions are switched to the crank-to-run mode until the run air predictor takes over. Details of misfire detection and recovery logic can be found in [10].

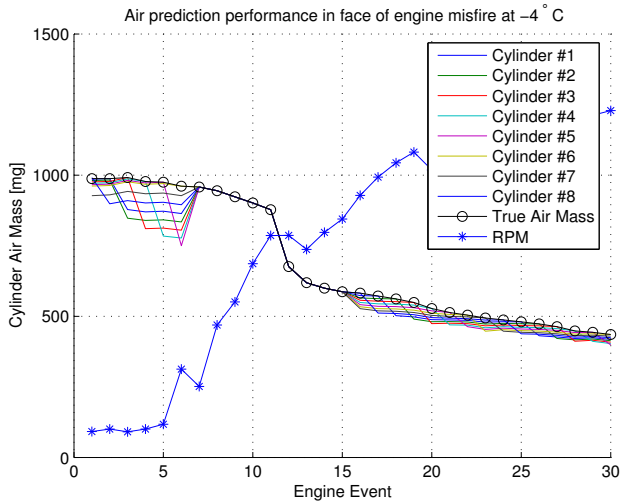


Fig. 12. Air Prediction in face of engine misfire: the first firing event occurs at event 6.

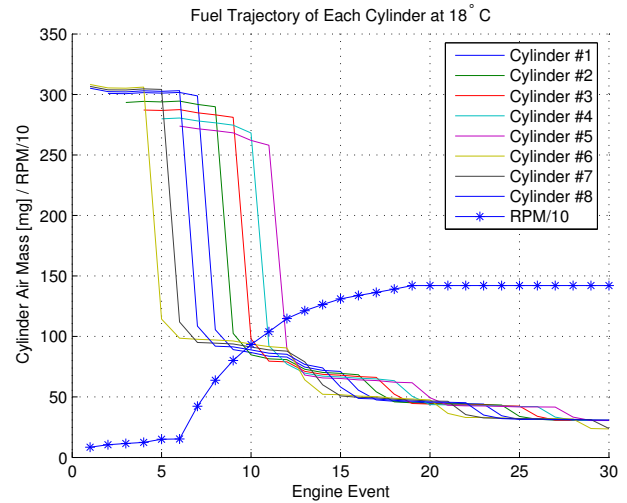


Fig. 14. Fuel trajectories under a good engine start: The first firing event occurs at event 7.

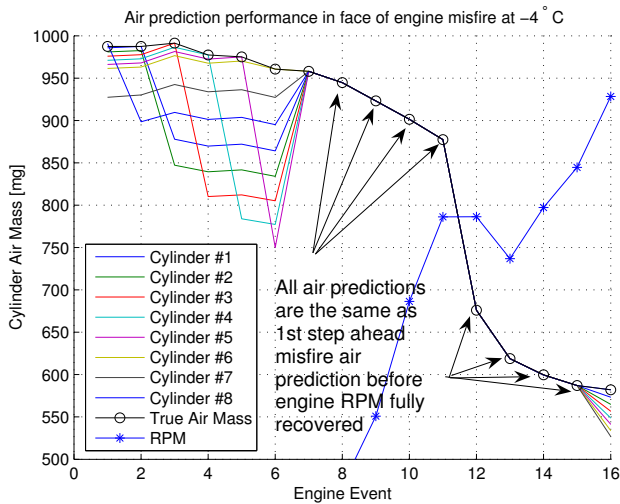


Fig. 13. Air Prediction in face of engine misfire: The first firing event occurs at event 6.

### B. Engine Start Performance

It is quite easy to understand that each cylinder requires different fuel commands during transient conditions such as start. Different fueling trajectories at the engine start condition for a multi-cylinder engine are shown in Figure 14.

The unique signature of individual cylinder fuel control is clearly depicted in Figure 14. More importantly, a fuel cycle footprint of each cylinder, such as switching from Cycle 1 to Cycle 2, can be clearly seen as well. This fine level of fuel control is not possible with the conventional controls, which "blend" crank and crank-to-run EQR's.

Another unique feature of this predictive fuel control is that the Cycle 2 fuel, in general, is much less than that from the static blending approach while still assuring robust engine start. This further demonstrates the benefit of model based control.

When misfire is detected (i.e., where the situation is the same as that shown in Figure 12), fuel trajectories as shown in Figure 15 are different from each other due to differences in fuel cycles.

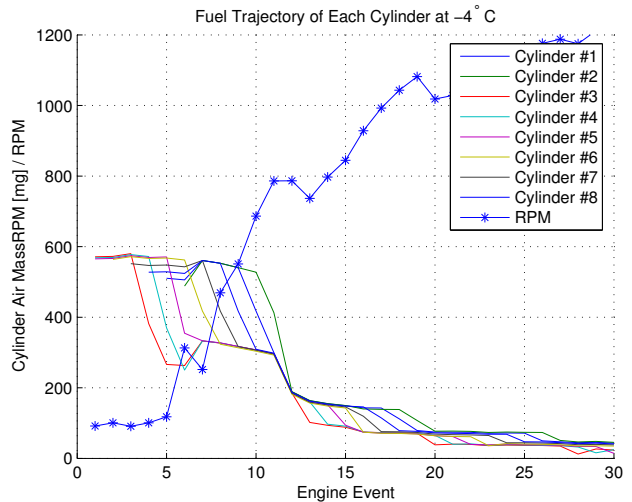


Fig. 15. Fuel trajectories in face of engine misfire: the first firing event occurs at event 6.

The close-up view, Figure 16, further explains why they are different. As shown, the fueling levels for all eight cylinders increase. This feature, systematically realized through the misfire air predictor provides an effective model-based method for misfire amelioration.

### C. Remark

Engine start results at only two ECTs have been presented. The scheme was, however, validated from  $-30^{\circ}\text{C}$  to hot temperatures (ECT). In addition, different soak times and two different types of fuel were tested on this scheme. These results will appear in a future paper.

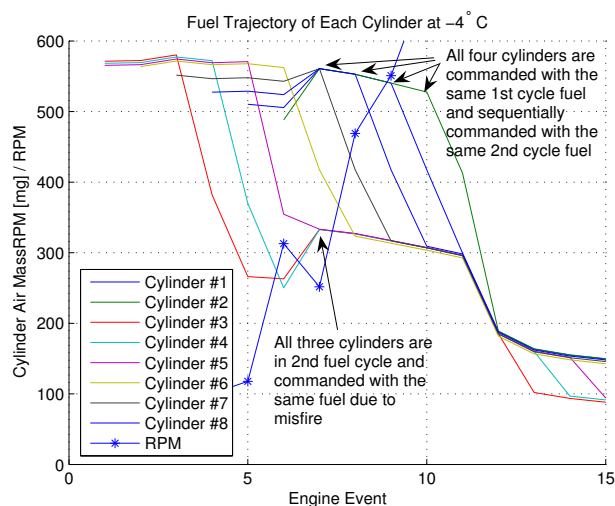


Fig. 16. Zoomed-in view of fuel trajectories in face of engine misfire.

### VIII. CONCLUSION

In this work, the engine start problem has been reviewed and discussed with respect to engine in-cylinder fresh air charge prediction and nonlinear fuel dynamics control. The synergy between cylinder air mass prediction and model-based open loop fuel dynamics control is revealed and demonstrated with experimental data. This work demonstrates that model-based, predictive fuel dynamics control, for engine start and crank-to-run transition, can be an effective production solution for PFI engines.

One of the primary contributions of this work lies in the reduction of control calibration effort. To date, control calibration schemes for the engine start, and crank-to-run transition problems, have required a significant amount of effort and associated cost, particularly considering the amount of calibration required for a wide range of temperatures. The control proposed (and validated) in this work requires significantly less effort in calibration, with the use of model-based control schemes and system identification techniques. Extension of these ideas to other control problems in automotive systems are underway.

### ACKNOWLEDGMENTS

The authors wish to acknowledge the tremendous help from Robert Shafto for his creative coding work to make the algorithm run on production controllers. In addition, the authors would like to thank Lee Walker for design of experiments and for supplying high quality engine start data.

### REFERENCES

[1] B. Bamieh and Laura Giarre. "Identification of Linear Parameter Varying Models". Proceedings of the Conference on Decision and Control, Dec. 1999.  
 [2] B. M. Castaing, J. S. Cowart, and W. K. Cheng. "Fuel Metering Effects on Hydrocarbon Emissions and Engine Stability During Cranking and Start-up in a Port Fuel Injected Spark Ignition Engine". Presented at the SAE International Fall Fuels and Lubricants Meeting and Exhibition, Mar. 2000. SAE Paper 2000-01-2836.

[3] A. Chevalier, C. W. Vigild, and E. Hendricks. "Predicting the port air mass flow of SI engines in air/fuel ratio control applications". Presented at the SAE International Congress and Exposition, Mar. 2000. SAE Paper 2000-01-0206.  
 [4] K. P. Dudek. "Application of Linear Splines to Internal Combustion Engine Control". US Patent No. 7, 212,915 B2., May. 2007.  
 [5] K. P. Dudek and C. H. Folkerts. "Method for Predicting R-Step Ahead Engine State Measurements". US. Patent No. 5,094,213, Mar. 1992.  
 [6] K. P. Dudek and V. A. White. "Engine with Prediction/Estimation Air Flow Determination". US. Patent No. 5,270,935, Dec. 1993.  
 [7] N. P. Fekete, N. Nester, I. Gruden, and J. D. Powell. "Model-based air-fuel ratio control of a lean multi-cylinder engine". Presented at the SAE International Congress and Exposition, Feb. 1995. SAE Paper 950846.  
 [8] K. R. Lang and W. K. Cheng. "Effect of Fuel Properties on First Cycle Fuel Delivery in a SI Engine". Presented at the SAE Powertrain and Fluid Systems Conference and Exhibition, Oct. 2004. SAE Paper 2004-01-3057.  
 [9] K. Leisenring, B. Samimy, and G. Rizzoni. "IC Engine Air/Fuel Ratio Feedback Control During Cold Start". Presented at the SAE International Congress and Exposition, Feb. 1996. SAE Paper 961022.  
 [10] Q. Ma. *Model Based Control and Efficient Calibration for Crank-to-Run Transition in SI Engines*. OSU dissertation, 2005.  
 [11] Q. Ma, S. Yurkovich, and K. P. Dudek. "Modeling of Nonlinear Fuel Utilization Phenomena During Engine Start and Crank-to-Run Transition". American Control Conference, Jun. 2006. Minneapolis, MN.  
 [12] Q. Ma, S. Yurkovich, and K. P. Dudek. "Cylinder Air Rate Prediction During Engine Start and Crank-to-Run Transition". American Control Conference, July 2007. New York City, USA.  
 [13] R. Meyer and J. B. Heywood. "Liquid Fuel Transport Mechanisms into the Cylinder of a Firing Port-Injected SI Engine during Start Up". Presented at the SAE International Congress and Exposition, Feb. 1997. SAE Paper 970865.  
 [14] H. Santoso and W. K. Cheng. "Mixture Preparation and Hydrocarbon Emissions Behaviors in the First Cycle of SI Engine Cranking". Presented at the SAE Powertrain and Fluid Systems Conference and Exhibition, Oct. 2002. SAE Paper 2002-01-2805.  
 [15] P. J. Shayler, R. M. Isaacs, and T. H. Ma. "The Variation of in-cylinder Mixture Ratio during Engine Cranking at Low Ambient Temperature". Proceedings of Institution of Mechanical Engineering, 1992. Vol. 206.  
 [16] R. H. Stanglmaier, M. J. Hall, and R. D. Matthews. "In-Cylinder Fuel Transport During the First Cranking Cycles in a Port Injected 4-Valve Engine". Presented at the SAE International Congress and Exposition, Feb. 1997. SAE Paper 970043.

### ACRONYM

- GPO** Cylinder air mass per event
- GPOM** Cylinder air mass measurement
- GPOF** Filtered cylinder air mass
- GPOE** Cylinder air mass estimate
- GPC** Cylinder air mass per event measured at throttle
- TPS** Throttle position signal
- MAP** Intake manifold absolute pressure
- RPM** Engine crankshaft speed
- SOC** Battery State of Charge
- ECT** Engine coolant temperature
- EQR** Equivalence ratio
- Toil** Engine oil temperature
- UFF** Utilized fuel fraction
- RINJ** Raw injected fuel mass
- CINJ** Lost fuel corrected raw injected fuel mass
- MBFM** Measured burned fuel mass
- CRK** Crank
- CTR** Crank to run